Journal of Power Sources 196 (2011) 5064–5069

Contents lists available at ScienceDirect

Journal of Power Sources

journal homepage: www.elsevier.com/locate/jpowsour

Solid oxide fuel cells with $Sm_{0.2}Ce_{0.8}O_{2-\delta}$ electrolyte film deposited by novel aerosol deposition method

Sea-Fue Wang*, Yung-Fu Hsu, Chih-Hao Wang, Chin-Ting Yeh

Department of Materials and Mineral Resources Engineering, National Taipei University of Technology, Taipei 10608, Taiwan, ROC

ARTICLE INFO

Article history:
Received 3 November 2010
Received in revised form 26 January 2011
Accepted 27 January 2011
Available online 2 February 2011

Keywords:
Solid oxide fuel cell
Ceria
Aerosol deposition
Electrolyte

ABSTRACT

In this study, dense electrolyte ceramic $Sm_{0.2}Ce_{0.8}O_{2-\delta}$ (SDC) thin films are successfully deposited on NiO-SDC anode substrate by aerosol deposition (AD) with oxygen as the carrier gas at the substrate temperature ranging from room temperature to 300 °C. To remove the effect of humidity on the starting powders, this study found that, in depositing SDC films, having the starting powders preheat-treated at 200 °C helped generate a smooth and dense layer, though a lower deposition rate was achieved. At a deposition time of 22 min, SDC films with a uniform thickness of 1.5 μm and grain sizes of ≈67 nm are obtained. SOFC single cells are then built by screen printing a LSCF cathode on the anode-supported substrates with SDC electrolyte. The cross-sectional SEM micrographs exhibit highly dense, granular, and crack-free microstructures. The open circuit voltages (OCV) of the single cells decrease with the rise in temperature, dropping from 0.81 V at 500 °C to 0.59 V at 700 °C. Maximum power densities (MPD) decline with decreasing operating temperature from 0.34 to 0.01 W cm^{-2} due to the increase of the R_0 and R_P of the single cells. The electrochemical results testify to the fine quality of SDC films as well as illustrate the electrolyte thickness effect and the effect of mixed ionic and electronic conduction of the SDC electrolyte in the reducing atmosphere.

1. Introduction

Solid oxide fuel cell (SOFC) system is considered to have superior potential for commercialization thanks to its high energy conversion efficiency, self-reforming ability, compatibility with common hydrocarbon fuels, use of solid state materials, and no need of noble metals as catalysts [1]. SOFC can be used in large-size stationary power facilities or applied to heat and power generation for homes and businesses as well as auxiliary power units for electrical systems in transportation vehicles. Planar-type SOFCs are superior to those with tubular designs because of their simple manufacturing process and promise of a high power density [2].

A conventional electrolyte-supported SOFC requires a minimum thickness of ≈150 μm for its electrolyte, and the thick electrolyte in turn demands an operating temperature around 900–1000 °C to minimize high-ohmic loss [3]. Such a high operating temperature implies poor long-term stability and places a stringent constraint on material selection; cost of materials, especially that of interconnect materials, can thus be fairly steep. In recent years, enormous research efforts have been invested on the development of intermediate temperature SOFCs (IT-SOFCs) capable of operating at temperatures between 500 and 700 °C [4]. However, the performance of IT-SOFCs depends to a substantial extent on the ionic conductivity of the electrolyte and the polarization resistance (R_P) of the electrodes [5]. The former problem can be solved by using alternative electrolytes with higher ionic conductivity at low temperatures, such as $La_{0.9}Sr_{0.1}Ga_{0.8}Mg_{0.2}O_{3-\delta}$ (LSGM) and $Sm_{0.2}Ce_{0.8}O_{2-\delta}$ (SDC) or by using a thin yttria-stabilized zirconia (YSZ) electrolyte film [6].

Several film-deposition methods have been used to reduce the thicknesses of electrolyte layers. These methods can be grouped into three categories: (a) physical approaches, including sputtering [7] and pulsed laser deposition (PLD) [8]; (b) chemical processes like sol–gel [9], spray pyrolysis [10], atomic layer deposition (ALD) [11], electrochemical vapor deposition (EVD) [12], metalorganic chemical vapor deposition (MOCVD) [13], flame assisted vapor deposition [14], and electrostatic assisted vapor deposition [15]; and (c) ceramic powder processes, such as screen printing [16], tape casting [17], suspension spray coating [18], slurry spin-coating [19], inject printing [20], electrophoretic deposition [21], and dry pressing [22]. However, these processes are often marked with restrictions that limit their applications, such as a high substrate temperature (typically around 700–900°C), sophisticated deposition and doping parameters, expensive precursors and processes, inhomogeneity in thickness, large induced strain, reliance on mul-

* Corresponding author. Present address: Department of Materials and Mineral Resources Engineering, National Taipei University of Technology, 1, Sec. 3, Chung-Hsiao E. Rd., Taipei 10608, Taiwan, ROC. Tel.: +886 2 2771 2171x2735; fax: +886 2 2731 7185.
E-mail addresses: sfwang@ntut.edu.tw, seafuewang@yahoo.com (S.-F. Wang).

0378-7753/$ – see front matter © 2011 Elsevier B.V. All rights reserved.
doi:10.1016/j.jpowsour.2011.01.083

tiple coatings, complex sintering procedures, and difficulty in stoichiometry control.

Recently, aerosol deposition (AD) method [23], a new deposition technique based on the collision of fine particles for fabrication and micropatterning of thick ceramic layers, has been developed. Successfully adopted to fabricate Pb(Zr,Ti)O_3, α-Al_2O_3, Y_2O_3, YSZ, AlN, MgB_2, and Ni–Cu–Zn ferrite ceramic thick films [23–30], AD method is effective for preparing ceramic films with a thicknesses over 1 μm due to its high deposition rate at temperatures below 100 °C; it enables us to achieve high density and easy control of stoichiometry and crystallinity. In this study, the feasibility of deposition of $Sm_{0.2}Ce_{0.8}O_{2-\delta}$ (SDC) films on NiO-SDC anode substrates by AD method from SDC powders was investigated. The crystal structure and microstructural evolution of the films were examined by X-ray diffraction (XRD) analysis and scanning electron microscopy (SEM). SOFC single cells were then built by screen printing a LSCF cathode on the anode-supported substrates with SDC electrolyte. Microstructural and electrochemical performance of the SOFCs were then characterized and discussed.

2. Experimental procedure

Commercially available raw materials for SOFC, including $Sm_{0.2}Ce_{0.8}O_{2-\delta}$ (SDC; Fuel Cell Materials, USA; d_{50} = 0.53 μm and BET surface area = 6.2 $m^2 g^{-1}$), $La_{0.6}Sr_{0.4}Co_{0.2}Fe_{0.8}O_{3-\delta}$ (LSCF: Fuel Cell Materials, USA; d_{50} = 0.99 μm and BET surface area = 5.4 $m^2 g^{-1}$), and NiO (anode functional layer: Fuel Cell Materials, USA, d_{50} = 0.8 μm and BET surface area = 3.4 $m^2 g^{-1}$; current collector layer: SHOWA, Japan, d_{50} = 10.1 μm and BET surface area = 0.06 $m^2 g^{-1}$), were used in this study. The anode substrates built were composed of a current collector layer (outer layer) of pure NiO and two functional layers of NiO-SDC composites with ratios of 60 wt%/40 wt% and 50 wt%/50 wt% respectively. Ceramic raw powders were mixed with 19.7 wt% of organic binder (B74001; Ferro), 25.6 wt% of solvent (60 wt% toluene/40 wt% ethanol) and 0.7 wt% of dispersant (M1201; Ferro) to form colloidal ceramic suspensions. The anode substrates were then built via tape casting process, and the dried and laminated tapes drilled into discs. 25 mm in diameter, the discs were co-fired at 1400 °C for 2 h at a heating rate of 2 °C min^{-1}.

A $Sm_{0.2}Ce_{0.8}O_{2-\delta}$ thick film was deposited on the anode substrates by AD method using $Sm_{0.2}Ce_{0.8}O_{2-\delta}$ powder. The AD apparatus is schematically shown in Fig. 1. $Sm_{0.2}Ce_{0.8}O_{2-\delta}$ powders were heat treated at 1300 °C for 4 h, ball milled in methyl alcohol solution using polyethylene jars with zirconia balls for 6 h, and subsequently oven dried at 80 °C for 30 h. The scanning electron microscopy (SEM; Hitachi S4700) image shown in Fig. 2 reveals a granular morphology of the powder particles. The powders report an average particle size of 1.08 μm, as measured by light scattering analyzer (Zeta 1000). The $Sm_{0.2}Ce_{0.8}O_{2-\delta}$ fine powders were placed in a flask (aerosol chamber), into which carrier gas of O_2 was introduced at the bottom of the powder bed to form an aerosol (suspension of fine ceramic particles in a carrier gas). The aerosol chamber was continuously vibrated so as to ensure thorough mixing of the ceramic particles with the accelerating gas. Aerosol flow from the aerosol chamber was subsequently transferred to the deposition chamber. Acceleration of the $Sm_{0.2}Ce_{0.8}O_{2-\delta}$ particles was driven by the pressure difference between the aerosol chamber and the deposition chamber. The high-speed moving particles then impinged upon, and were thus deposited onto, the Pt/Ti-buffered Si substrates placed 10 cm underneath the nozzle. The typical parameters adopted are listed in Table 1. To obtain uniform thickness across a large area, the substrates were placed on an X–Y stage and scanned over a 12 mm × 12 mm area at the speeds of 1.5 mm s^{-1} in the X direction and 1.5 mm s^{-1} in the Y direction back and forth

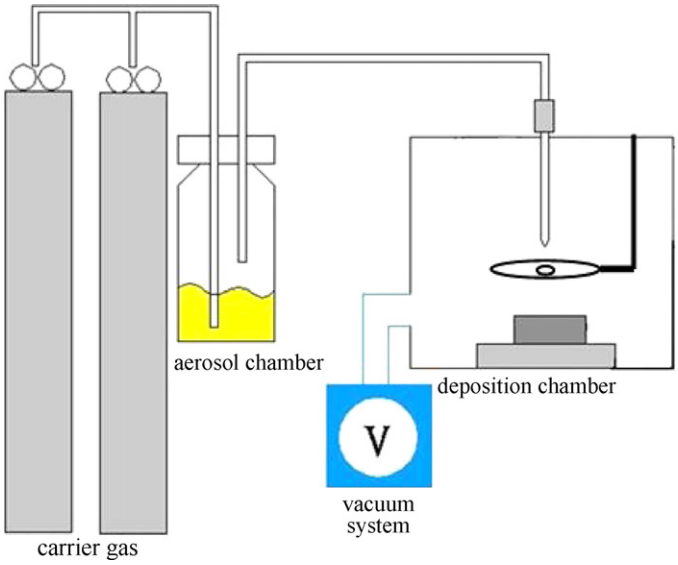

Fig. 1. Schematic of AD apparatus.

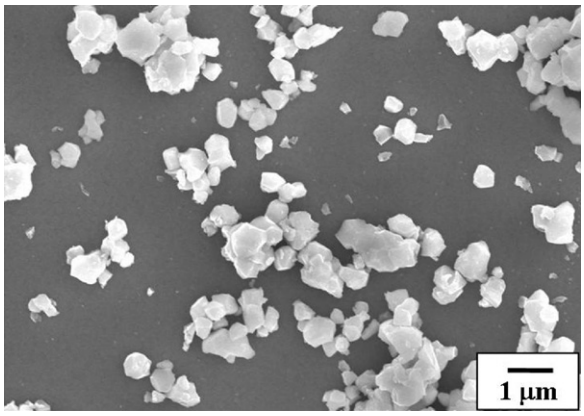

Fig. 2. SEM micrograph of the initial $Sm_{0.2}Ce_{0.8}O_{2-\delta}$ powder.

in the manner of meandering lines. During the process of deposition, the substrate holder was controlled at temperatures ranging from room temperature to 300 °C. X-ray diffraction (XRD) analysis, scanning electron microscopy (SEM), and energy dispersive spectroscopy (EDS) were used to confirm the formation of phases and to characterize the microstructures of films.

The anode-supported substrates with a SDC electrolyte layer deposited by AD method and a three-layer anode built via tape casting process were then screen printed to form a LSCF cathode. The LSCF cathode was prepared by screen-printing a LSCF material on the anode-supported SDC substrate (Fig. 3). Cathode powders were mixed with a proper amount of terpineol (solvent) and ethyl cellulose (binder) to form a paste. The cathode was then fired at 1000 °C

Table 1
Typical process conditions of the adopted aerosol deposition.

Deposition pressure (torr)	2–20
Aerosol chamber pressure (torr)	350–700
Nozzle orifice (mm)	1.1
Carrier gas	O_2
Flow rate of carrier gas (L min^{-1})	5
Substrate temperature	300 °C
Deposition area (mm^2)	22 × 22
Scan speed (mm s^{-1})	1.0
Nozzle/substrate distance (mm)	10

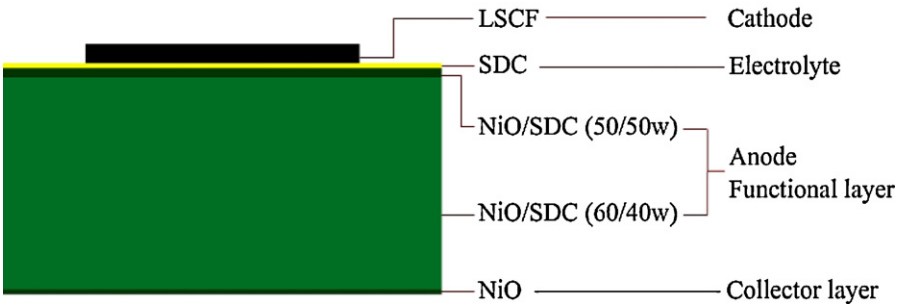

Fig. 3. Schematic drawing of the anode-supported single cell structure of SOFC with a $Sm_{0.2}Ce_{0.8}O_{2-\delta}$ electrolyte layer deposited by AD method.

for 2 h. Table 2 shows the dimensions of the single cell prepared in this study.

The electrochemical performance of the single cell was measured at the set-up of a commercially available ProboStat (NorECs, Norway). The cell was heated up to 1000 °C under nitrogen atmosphere (0.0338 Pa $m^3 s^{-1}$) on both sides of the cell for a gas-tight seal. The temperature was then reduced to 500 °C for anode reduction under hydrogen atmosphere before electrochemical measurements. During testing, the flow rates of hydrogen (3% H_2O) and air were kept respectively at 0.0676 and 0.2704 Pa $m^3 s^{-1}$ by electronic mass flow controllers. The current density as a function of cell voltage (*I–V* curves) was evaluated under different applied loads across the cell, and measurements were carried out at 500–700 °C at an interval of 50 °C. Electrochemical impedance spectra (EIS) were measured after holding the cells under OCV for 15 min at each temperature. The EIS measurements were performed with a four-lead two-electrode configuration using a multi-channel Potentiostat/Galvanostat (Solartron 1470E) and a 1260 frequency response analyzer with a computer interface and Corr-view software. The frequency ranged from 10^5 Hz to 0.015 Hz while the signal amplitude read 10 mV. *I–V* curves and power curves were obtained using linear sweep from OCV to 0.2 V at a sweep rate of 5 mV s^{-1}. After testing, the microstructure of the cells was examined by SEM (Hitachi S4700).

3. Results and discussion

Ceramic films fabricated by aerosol deposition methods requires precise control of process parameters, including the characteristics of starting powders, carrier gases, substrate temperature, and substrate characteristics, in order to obtain desired film properties [23]. The study attempted to deposit $Sm_{0.2}Ce_{0.8}O_{2-\delta}$ (SDC) films on anode substrates consisting of three layers with a total thickness of approximately 0.66 mm, including a current collector layer of NiO (≈20 μm) and two functional composite layers (with NiO/SDC ratios of 60/40 wt% and 50/50 wt%, and thicknesses of ≈636 μm and ≈6 μm respectively, as indicated in Table 2). The process was optimized using the carrier gas of O_2, the substrate temperature of 300 °C, and other essential process parameters listed in Table 1. In addition to the parameters which have been observed in the literature [23–30] as affecting AD deposition, this study found the quality of SDC films prepared using AD method highly sensitive to the relative humidity of the environment during deposition. High water absorption on the powder surface easily leads to powder agglomeration and affects the particle jet flow near the substrate. Preheat-treatment of the starting powder was therefore undertaken to remove water absorption. Fig. 4(a) and (b) shows the SEM micrographs of the anode-supported single cell structure of the SOFC with $Sm_{0.2}Ce_{0.8}O_{2-\delta}$ (SDC) electrolyte layer deposited by AD method after electrochemical measurements, using the starting powder without and with preheat-treatment at 200 °C, respectively. After a deposition time of approximately 22 min, the thickness of SDC film prepared using starting powder without preheat treatment read ≈25 μm [Fig. 4(a)], which was much thicker than that (1.5 μm) of its counterpart with preheat treatment at 200 °C [Fig. 4(b)]. Moreover, the former demonstrated an uneven and loose microstructure while the later reported a very uniform and dense microstructure.

Table 2
Design of the anode-supported single SOFC cells with a SDC electrolyte layer deposited by AD method.

Structure	Material	SOFC cell
Cathode current collector layer	LSCF	40 μm
Electrolyte layer	SDC	1.5 μm
Anode functional layer	NiO/SDC(50 wt%/50 wt%)	6 μm
Anode functional layer	NiO/SDC(60 wt%/40 wt%)	636 μm
Anode current collector layer	NiO	20 μm

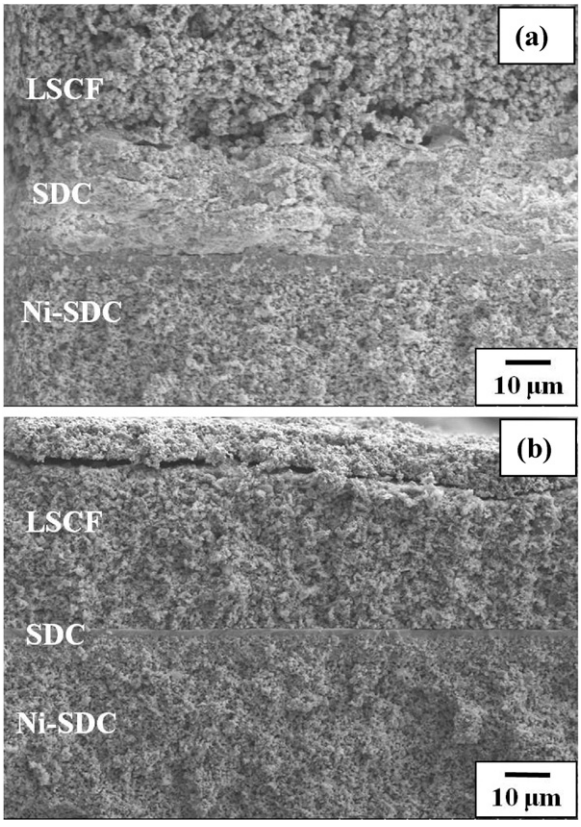

Fig. 4. SEM micrographs of the anode-supported single cell structure of the SOFC with $Sm_{0.2}Ce_{0.8}O_{2-\delta}$ electrolyte layer deposited by AD method using the starting powder (a) without and (b) with preheat-treatment at 200 °C.

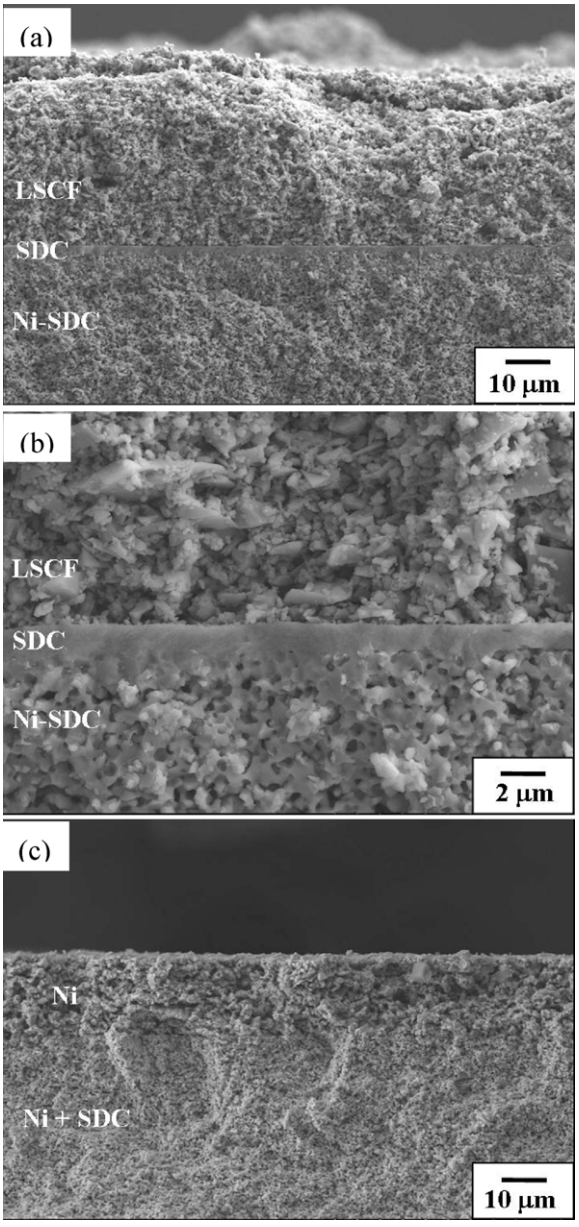

Fig. 5. Cross-sectional view of SEM images of the (a) cathode, (b) $Sm_{0.2}Ce_{0.8}O_{2-\delta}$ films deposited by AD, and (c) anode.

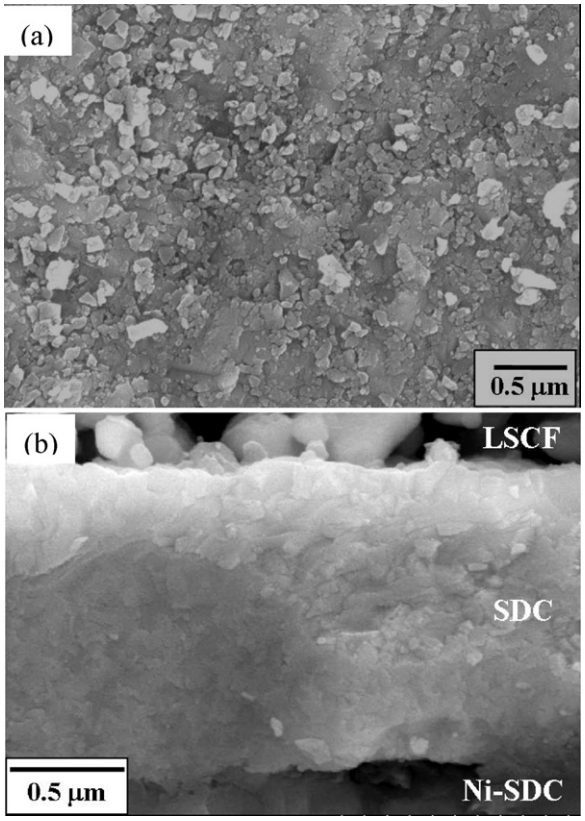

Fig. 6. (a) Cross-section and (b) surface SEM images of $Sm_{0.2}Ce_{0.8}O_{2-\delta}$ electrolyte films deposited by AD method.

Fig. 5 shows the SEM micrographs of the anode-supported single cell structure of the SOFC with $Sm_{0.2}Ce_{0.8}O_{2-\delta}$ (SDC) electrolyte layer deposited by AD method after electrochemical measurements. The interfaces among the anode, electrolyte, and cathode layers showed no sign of crack, discontinuity, or delamination. XRD analysis confirmed the complete reduction of NiO to Ni at the anode after the electrochemical test. Both the anode and cathode layers were marked with the presence of porous microstructures. As shown in Fig. 6(a), the observation of surface microstructure reveals that the SDC film has fine grain microstructures. The grain size of the SDC film is approximately 67 nm with a round morphology. The cross-sectional micrographs exhibit dense and granular microstructures [Fig. 6(b)]. The film shows a fairly uniform thickness of approximately 1.5 μm. It can be observed that the SDC electrolyte deposited by aerosol deposition in carrier gas of oxygen is crack free and dense to allow no passage for gas leakage in the SOFC electrolyte. Lamellar structure, which is observed in the TiO_2/Al_2O_3 film in the literature [30], is absent in the SDC film. In agreement with the densification mechanism proposed by Akedo [27], the grain sizes of the films are much smaller than the particle size of the starting SDC powder (1.08 μm; Fig. 2). The starting particles were accelerated in a gas jet to moderate velocities of 100–600 m s^{-1}. They were fractured into smaller fragments and deformed to fill the gaps between the deposited particles during impact with the substrate. No additional post annealing is required for solidification and densification after deposition. Moreover, as indicated in Fig. 5, the anode-supported SOFC with a SDC electrolyte layer deposited by AD apparently sustains good adhesion at the interfaces among the layers to ensure good integrity of the cell.

Fig. 7 shows the XRD patterns respectively of the initial SDC powders, the as-deposited SDC film by aerosol deposition in carrier gas of oxygen, and the film after annealing at 1000 °C. The diffraction peaks of the XRD patterns of the initial powders are indexed to the cubic $Fm\bar{3}m$ structure of $Sm_{0.2}Ce_{0.8}O_{2-\delta}$ (JCPDS Card No. 75-0158, $a = 0.5433$ nm). The as-deposited film was well-crystalline, and the broad multiple peaks further indicate fine grains and random orientation microstructure. No additional phases are detected in the films. The XRD patterns of the film after annealing are similar to those of the as-deposited film, implying that the subsequent cathode firing at 1000 °C did not change the phase structure and crystallinity of the SDC film in the anode-supported SOFC and verifying thereby the formation of good quality SDC film obtained in as-deposited form.

Fig. 8 shows the Nyquist plots of the electrochemical impedance spectra of the single cell containing a SDC electrolyte layer prepared by AD method. The highest frequency intercept of the impedance spectra gives the total ohmic resistance of the cell (R_0), including the resistive contributions of the electrolyte, the two electrodes, the current collectors, and the lead wires. The lowest frequency intercept gives the overall resistance of the cell, and the distance

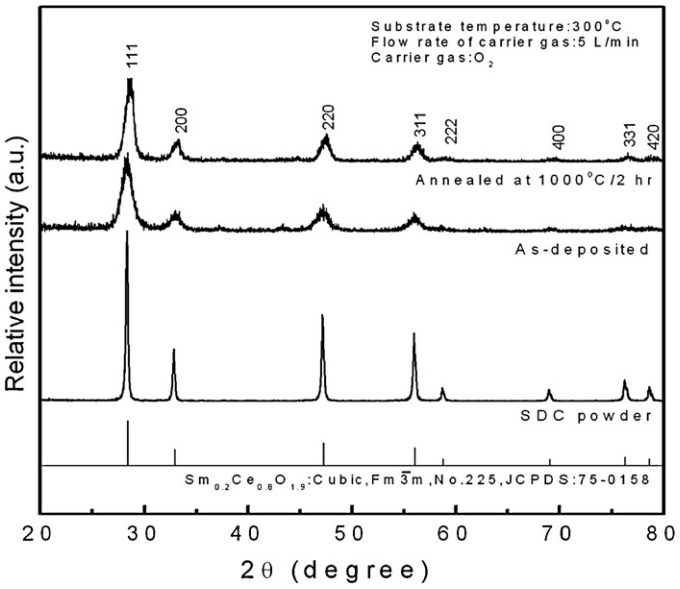

Fig. 7. XRD patterns of the initial $Sm_{0.2}Ce_{0.8}O_{2-\delta}$ powders, the as-deposited film, and the film annealed at 1000 °C.

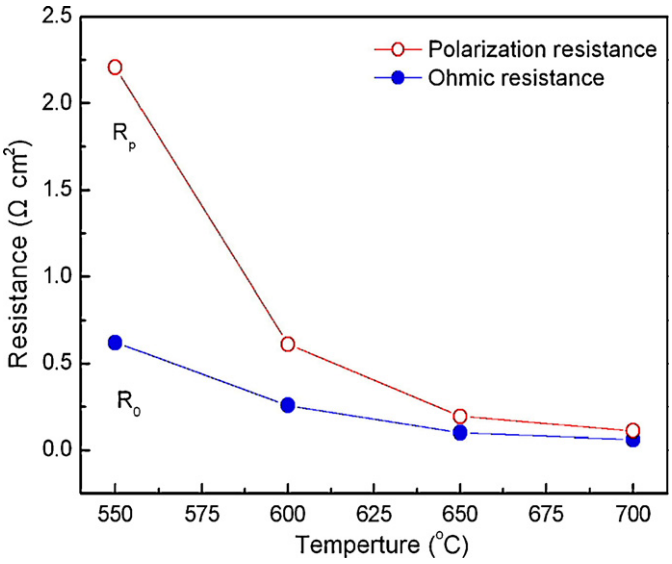

Fig. 9. Temperature dependences of ohmic resistances (R_0) and polarization resistances (R_P) of the anode-supported single cells containing a $Sm_{0.2}Ce_{0.8}O_{2-\delta}$ electrolyte layer deposited by AD.

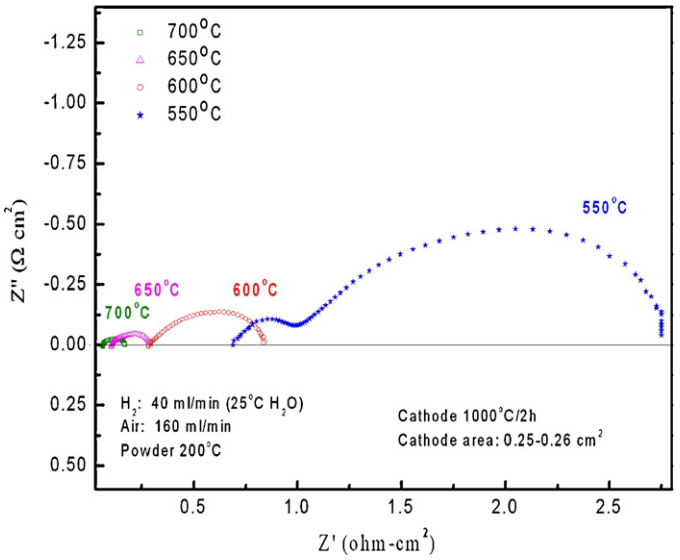

Fig. 8. Impedance spectra of the anode-supported single cells containing a $Sm_{0.2}Ce_{0.8}O_{2-\delta}$ electrolyte layer deposited by AD, at different temperatures.

between the two intercepts corresponds to the total interfacial polarization resistance (R_P) [31]. Fig. 9 presents the temperature dependence of R_0 and R_P of the single cells, and Table 3 lists the results. It can be observed that the R_0 of the single cells increased continuously from 0.060 to 0.62 Ω-cm^2 as the measurement temperature went down from 700 °C to 550 °C, a typical occurrence due to the dependence of the ionic conductivity of the SDC on temperature. The SDC content at both the electrolyte layer and the Ni-SDC anode layer may serve as the major cause of the rising R_0. It is evident from Fig. 8 that R_P rose as the temperature dropped, particularly at temperatures ≤600 °C. It should be noted that the contribution of R_0 to the total resistance ($R_{tot} = R_0 + R_P$) is small due to the thinner electrode layer (1.5 μm). The ratio of R_0 to R_{tot} read approximately 35% at 700 °C and decreased dramatically as the operating temperature was reduced (<22% at 550 °C), suggesting the fine quality of the SDC electrolyte film prepared by AD method and, therefore, the cell performance replies critically on the polarization resistance of the electrode.

Figs. 10 and 11 present respectively the cell performance as a function of the operating temperature, and the temperature dependences of open circuit voltage (OCV) and the maximum power density (MPD) of the anode-supported SOFC with a SDC electrolyte deposited by AD method. The SDC electrolyte layer possessed a higher electronic conduction that led to a lower OCV at high temperature, and the cells reported a higher degree of concentration polarization at high temperature as indicated by the convex-up curvature of the *I–V* curves at high current densities as shown in

Table 3
Results of R_0 and R_P electrochemical impedance spectra of the anode-supported single cell measured at temperatures ranging from 550 °C to 700 °C.

Temperature (°C)	R_0 (Ω-cm^2)	R_P (Ω-cm^2)	$R_0/(R_0+R_P)$
700	0.060	0.110	0.353
650	0.100	0.194	0.340
600	0.258	0.611	0.297
550	0.620	2.206	0.219

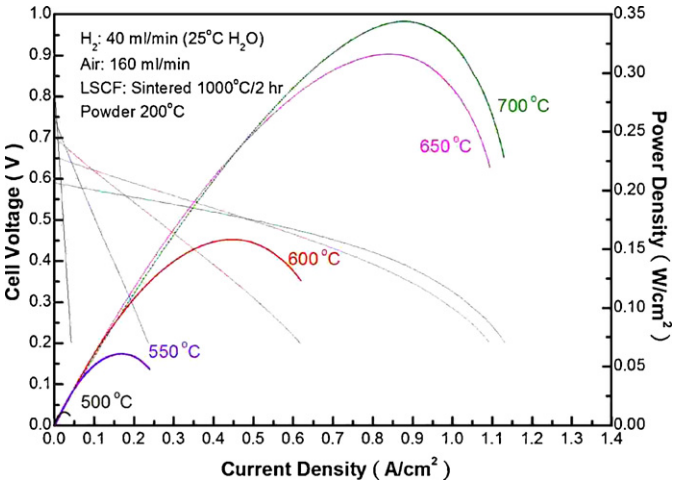

Fig. 10. *I–V* curves and the corresponding power densities of the anode-supported single cells containing a $Sm_{0.2}Ce_{0.8}O_{2-\delta}$ electrolyte layer deposited by AD, at different temperatures.

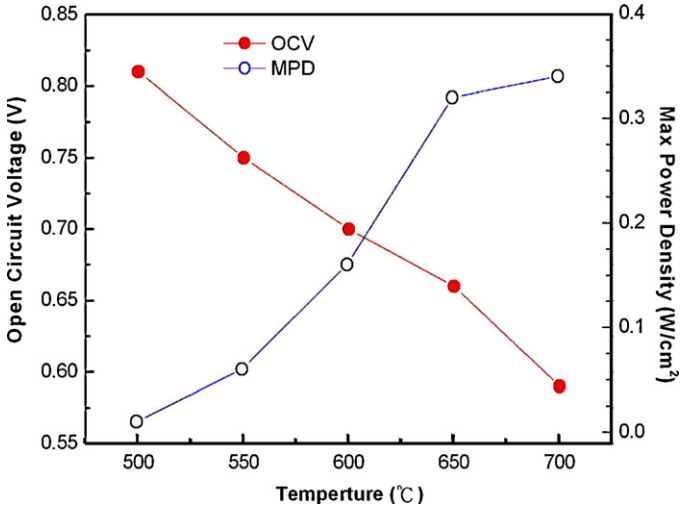

Fig. 11. Temperature dependences of OCV and maximum power density of the anode-supported single cells containing a $Sm_{0.2}Ce_{0.8}O_{2-\delta}$ electrolyte layer deposited by AD, at different temperatures.

Fig. 10. The OCV of the single cell decreased with the rise in temperature, dropping from 0.81 V at 500 °C to 0.59 V at 700 °C. These OCV values are lower than the expected theoretical values at higher temperatures because of the mixed ionic and electronic conduction of the SDC electrolyte in the reducing atmosphere [6]. Part of the Ce^{4+} ions in the electrolyte were reduced to Ce^{3+} ions, causing some electronic conduction in the electrolyte and resulting in OCV drop. With decreasing temperature, OCV gradually moved up as the electronic conduction went down at lower temperatures. In addition, the very thin electrolyte layer (1.5 μm, as shown in Fig. 5) led to dramatic decrease in OCV with rising temperature. Maximum power densities (MPD) declined with decreasing operating temperature from 0.34 to 0.01 W cm^{-2} due to the increase of the R_0 and R_P of the single cells as shown in Fig. 8. Both the OCV and MPD of the single cell prepared in this study are lower than those reported in the literature for the SOFCs with an electrolyte thickness greater than 10 μm. As reported by Ding et al., both the OCV and MPD of the anode-supported single cell significantly decreases with reduced thickness of the $Gd_{0.1}Ce_{0.9}O_{1.95}$ (GDC) electrolyte films when the thickness of the electrolyte films is less than approximately 5 μm. The decrease of the MPD may be due to the fact that the effect of the increase in electronic conduction of the GDC thin films on the electrical performance is greater than the effect of the decrease in ohmic-resistance loss resulted from the thin electrolyte layer [32].

4. Conclusions

In this study, anode-supported planar IT-SOFCs with a thin SDC electrolyte film were fabricated using AD method. Major conclusions reached by the study are summarized as follows:

(a) Using a preheat-treated starting powder and at a deposition time of 22 min, the obtained SDC electrolyte with a thickness of approximately 1.5 μm appeared to be crack free and very dense. The interfaces among the anode, electrolyte, and cathode layers for all cells showed good adhesion.

(b) The grain size of the film (67 nm) was much smaller than the particle size of the starting SDC powder (1.08 μm). No additional post annealing was required for solidification and densification after deposition. The XRD patterns of the as-deposited film confirmed the well-crystalline fine grains and random orientation microstructure. No additional phases were detected in the films.

(c) The open circuit voltage (OCV) of the single cell dropped from 0.81 V to 0.59 V while the maximum power densities (MPD) escalated from 0.01 to 0.34 W cm^{-2} as the operating temperature increased from 500 °C to 700 °C.

References

[1] M.D. Mata, X. Liub, Z. Zhu, B. Zhu, Int. J. Hydrogen Energy 32 (2007) 796–801.
[2] T.L. Wen, D. Wang, M. Chen, H. Tu, Z. Lu, Z.R. Zhang, H. Nie, Solid State Ionics 148 (2002) 513–519.
[3] J.H. Joo, G.M. Choi, J. Power Sources 180 (2008) 195–198.
[4] E. Ivers-Tiffée, A. Weber, D. Herbstritt, J. Eur. Ceram. Soc. 21 (2001) 1805–1811.
[5] M. Zhang, M. Yang, Z. Hou, Y. Dong, M. Cheng, Electrochim. Acta 53 (2008) 4998–5006.
[6] J.W. Fergus, J. Power Sources 162 (2006) 30–40.
[7] N. Jordan, W. Assenmacher, S. Uhlenbruck, V.A.C. Haanappel, H.P. Buchkremer, D. Stover, W. Mader, Solid State Ionic 179 (2008).
[8] D. Yang, X. Zhang, S. Nikumb, C. Deces-Petit, R. Hui, R. Maric, D. Ghosh, J. Power Sources 164 (2007) 182–188.
[9] Z. Zao, J. Huang, Z. Mao, C. Wang, Z. Liu, Int. J. Hydrogen Energy 35 (2010) 731–737.
[10] L. Liu, G.Y. Kim, A. Chandra, J. Power Sources 195 (2010) 7046–7053.
[11] C.C. Chou, Y.B. Kim, F.B. Prinz, Nano Lett. 9 (2009) 3626–3628.
[12] A. Mineshige, K. Fukushima, K. Tsukada, M. Kobune, T. Yazawa, K. Kikuchi, M. Inaba, Z. Ogumi, Solid State Ionics 175 (2004) 483–485.
[13] A. Tarancon, N. Sabate, A. cavallaro, I. Gracia, J. Roqueta, I. Garbayo, J.P. Esquivel, G. Garcia, C. Cane, J. Santiso, J. Nanosci. Nanotechnol. 10 (2010) 1327–1337.
[14] S. Charoirochkul, R.M. Rothian, K.L. Choy, B.C.H. Steele, J. Eur. Ceram. Soc. 24 (2004) 2527–2535.
[15] J. Yan, X. Hou, K.L. Choy, J. Power Sources 180 (2008) 373–379.
[16] X. Zhang, M. Robertson, C. Deces-Petit, Y. Xie, R. Hui, W. Qu, O. Kesler, R. Maric, D. Ghsoh, J. Power Sources 175 (2008) 800–805.
[17] H. Moon, S.D. Kim, S.H. Hyun, H.S. Kim, Int. J. Hydrogen Energy 33 (2008) 1758–1768.
[18] Y.J. Leng, S.H. Chan, K.A. Khor, S.P. Jiang, Int. J. Hydrogen Energy 29 (2004) 1025–1033.
[19] K. Chen, Y. Tian, A. Lu, N. Ai, X. Huang, W. Su, J. Power Sources 186 (2009) 128–132.
[20] R.I. Tomova, M. Krauz, J. Jewulski, S.C. Hopkins, J.R. Kluczowski, D.M. Glowacka, B.A. Glowacki, J. Power Sources 195 (2010) 7160–7167.
[21] M. Matsuda, T. Hosomi, K. Murata, T. Fukui, M. Miyake, J. Power Sources 165 (2007) 102–107.
[22] Q. Ma, J. Ma, A. Zhou, R. Yan, J. Gao, G. Meng, J. Power Sources 164 (2007) 86–89.
[23] J. Akedo, J. Therm. Spray Technol. 17 (2008) 181–198.
[24] J. Akedo, M. Lebedev, Recent Res. Dev. Mater. Sci. 2 (2001) 51–77.
[25] J. Akedo, M. Kiyohara, J. Soc. Powder Technol. Jpn. 40 (2003) 192–201.
[26] J. Akedo, Mater. Sci. Forum (2004) 449–452.
[27] J. Akedo, M. Lebedev, Jpn. J. Appl. Phys. 38 (1999) 5397–5401.
[28] J. Akedo, J. Am. Ceram. Soc. 89 (2006) 1834–1839.
[29] M. Lebedev, J. Akedo, T. Ito, J. Crystal Growth 275 (2005) e1301–1306.
[30] Y. Imanaka, M. Takenouchi, J. Akedo, J. Crystal Growth 275 (2005) e1313–1319.
[31] H.C. Yu, F. Zhao, A.V. Virkar, K.Z. Fung, J. Power Sources 152 (2005) 22–26.
[32] C. Ding, H. Lin, K. Sato, K. Amezawa, T. Kawada, J. Mizusaki, T. Hashida, J. Power Sources 195 (2010) 5487–5492.